

~~CONFIDENTIAL~~

Copy
RM L50H16

NACA RM L50H16

~~NOTE~~

2.1

NACA

RESEARCH MEMORANDUM

FLIGHT MEASUREMENTS WITH THE DOUGLAS D-558-II

(BUAERO NO. 37974) RESEARCH AIRPLANE

MEASUREMENTS OF WING LOADS AT MACH NUMBERS UP TO 0.87

By John P. Mayer, George M. Valentine,
and Beverly J. Swanson.

FOR REFERENCE

Langley Aeronautical Laboratory
Langley Field, Va.

UNCLASSIFIED

NOT TO BE TAKEN FROM THIS ROOM

To _____

By authority of TRCARS also effective
FRN-128 Date Jan 24, 1958
AMT 8-12-58

CLASSIFIED DOCUMENT

This document contains classified information affecting the National Defense of the United States within the meaning of the Espionage Act, USC 50-81 and 82. Its transmission or the revelation of its contents in any manner to an unauthorized person is prohibited by law. Information so classified may be imparted only to persons in the military and naval services of the United States, appropriate civilian officers and employees of the Federal Government who have a legitimate interest therein, and to United States citizens of known loyalty and discretion who if necessary must be informed thereof.

NATIONAL ADVISORY COMMITTEE FOR AERONAUTICS

WASHINGTON
December 26, 1950

~~CONFIDENTIAL~~



NATIONAL ADVISORY COMMITTEE FOR AERONAUTICS

RESEARCH MEMORANDUM

FLIGHT MEASUREMENTS WITH THE DOUGLAS D-558-II

(BUAERO NO. 37974) RESEARCH AIRPLANE

MEASUREMENTS OF WING LOADS AT MACH NUMBERS UP TO 0.87

By John P. Mayer, George M. Valentine,
and Beverly J. Swanson

SUMMARY

Flight measurements have been made of the aerodynamic wing normal force, bending moment, and pitching moment by means of strain gages on the D-558-II airplane at Mach numbers up to 0.87 and at angles of attack up to 38° for low Mach numbers. These measurements indicate that the wing normal-force-curve slope is approximately 8 percent less than the airplane normal-force-curve slope at Mach numbers up to 0.87 principally because of the normal force contributed by the fuselage. The spanwise center of pressure of additional air load on the wing was found to be unaffected by Mach number for Mach numbers up to 0.87. The aerodynamic center of the wing moved forward slightly as the Mach number increased up to 0.80. From a Mach number of 0.80 to 0.87 the wing aerodynamic center moved rearward. The aerodynamic center of the fuselage moved rearward throughout the Mach number range covered in these tests; this movement indicates that a large part of the increase in airplane stability at Mach numbers up to 0.80 is caused by the increase in fuselage stability with Mach number. For low Mach numbers the center of pressure on the wing moved inboard and rearward at high angles of attack for the slats-locked configuration. For the slats-unlocked configuration the center of pressure moved rearward and gradually outboard at angles of attack up to 23° . At an angle of attack near 23° the center of pressure shifted rapidly inboard and forward somewhat and then remained approximately constant at angles of attack up to 38° . The investigation showed that the wing did not cause the longitudinal instability of the airplane at high normal-force coefficients since the wing became increasingly stable in the angle-of-attack range for which the airplane is unstable.

INTRODUCTION

As part of the cooperative NACA-Navy transonic flight research program, the National Advisory Committee for Aeronautics is utilizing the Douglas D-558-II research airplane for flight investigations at the NACA High-Speed Flight Research Station at Edwards Air Force Base, Calif. This paper presents results from the measurements of wing loads by means of strain gages in the Mach number range from 0.37 to 0.87. From these measurements were determined the variations with Mach number of the additional air load spanwise center of pressure, the aerodynamic center of the wing, and the normal-force-curve slope of the wing. In addition, the variation of spanwise and chordwise center of pressure with airplane angle of attack and normal-force coefficient were determined.

Results on other aerodynamic characteristics of the D-558-II airplane have been presented in references 1 to 6.

SYMBOLS

a	velocity of sound, feet per second
a.c.	aerodynamic center
EM_{WP}	wing-panel bending moment about wing station 33 inches, foot pounds
$\frac{b_{WP}}{2}$	span of wing panel, 9.75 feet
C.P.A	spanwise center of pressure of the additional air load in percent of the span of the wing panel
C.P.x	chordwise center of pressure in percent of mean aerodynamic chord of wing panel
C.P.y	spanwise center of pressure in percent of span of wing panel
C_M	pitching-moment coefficient
$C_{M_{\bar{c}}/4}$	wing-panel pitching-moment coefficient about the quarter chord of the complete wing mean aerodynamic chord $\left(\frac{PM_{WP}}{qS_W/2\bar{c}} \right)$

$C_{M_{WP}} \bar{c}_{WP}/4$	wing-panel pitching-moment coefficient about the quarter chord of the wing-panel mean aerodynamic chord $\left(\frac{PM_{WP}}{qS_{WP} \bar{c}_{WP}} \right)$
$C_{B_{WP}}$	wing-panel bending-moment coefficient $\left(\frac{BM_{WP}}{qS_{WP} b_{WP}/2} \right)$
C_N	normal-force coefficient
C_{N_A}	airplane normal-force coefficient $\left(\frac{nW}{qS_W} \right)$
$C_{N_{WF}}$	wing-fuselage normal-force coefficient
$C_{N_{WP}}$	wing-panel normal-force coefficient $\left(\frac{L_{WP}}{qS_{WP}} \right)$
$\bar{c}, M.A.C.$	mean aerodynamic chord of complete wing, 87.301 inches
\bar{c}_{WP}	mean aerodynamic chord of wing panel, 81.334 inches
d_s	slat position, inches open
g	acceleration due to gravity, feet per second ²
L_{WP}	aerodynamic wing-panel load, pounds
n	airplane normal-load factor
PM_{WP}	left-wing-panel pitching moment, foot pounds
q	dynamic pressure, pounds per square foot $\left(\frac{\rho V^2}{2} \right)$
M	free-stream Mach number (V/a)
S_W	wing area, 175 square feet
S_{WP}	wing-panel area outboard of wing station at 33 inches, 63.8 square feet
V	free-stream velocity, feet per second
W	airplane gross weight, pounds
x	distance measured from leading edge of the mean aerodynamic chord parallel to airplane center line

- y distance measured from the strain-gage station perpendicular to airplane center line
- α_A airplane angle of attack (measured with respect to airplane center line), degrees
- ρ mass density of air, slugs per cubic foot
- δ_e elevator angle, degrees

Subscripts:

- A airplane
- F fuselage
- W complete wing
- WP wing panel outboard of strain-gage station
- WF wing-fuselage combination

AIRPLANE

The Douglas D-558-II airplanes have sweptback wing and tail surfaces and were designed for combination turbojet and rocket power plant. The airplane being used in the present investigation (BuAero No. 37974) does not have the rocket engine installed. This airplane is powered by a J-34-WE-40 turbojet engine which exhausts out of the bottom of the fuselage between the wing and the tail. Both slats and stall-control vanes are incorporated on the wing of the airplane. The wing slats can be locked in the closed position or they can be unlocked. When the slats are unlocked, the slat position is a function of the angle of attack of the airplane. The airplane is equipped with an adjustable stabilizer. Photographs of the airplane are shown in figures 1 and 2 and a three-view drawing is shown in figure 3. A drawing of the wing section showing the wing slat in the closed and extended position is given in figure 4. Pertinent airplane dimensions and characteristics are listed in table 1.

INSTRUMENTATION AND ACCURACY

Standard NACA instruments are installed in the airplane to measure the following quantities:

- Airspeed
- Altitude
- Elevator and aileron wheel force
- Rudder-pedal force
- Normal, longitudinal, and transverse accelerations at the center of gravity of the airplane
- Normal, longitudinal, and transverse accelerations at the tail
- Pitching, rolling, and yawing velocities
- Airplane angle of attack
- Stabilizer, elevator, rudder, aileron, and slat positions

Strain gages are installed on both sides of the wing and horizontal tail to measure wing loads at the wing station at 33 inches from the airplane center line and horizontal tail loads at the station 6 inches from the airplane center line. A schematic drawing showing the strain-gage locations is presented in figure 5. The strain-gage circuits operate on direct current and the outputs of the strain gages were recorded on an 18-channel recording oscillograph. The strain gages were calibrated in terms of loads by applying known loads at many points on the structure. The measured outputs of the gages were utilized to obtain equations from which the load could be found from the gage responses during flight. In flight, the strain gages respond to a combination of aerodynamic and inertia loads. The loads given in this paper have been corrected for inertia effects and represent aerodynamic loads.

A free-swiveling airspeed head was used to measure both static and total pressures. This airspeed head was mounted on a boom approximately 7 feet forward of the nose of the airplane. The vane which was used to measure angle of attack was mounted below the same boom approximately $4\frac{1}{2}$ feet forward of the nose of the airplane.

The airspeed system was calibrated for position error by making tower passes at Mach numbers from 0.30 to 0.70 and at the normal-force coefficients for level flight. The free-swiveling airspeed head used on the airplane was calibrated in a wind tunnel for instrument error at Mach numbers up to 0.85. Tests of similar nose-boom installations indicate that the position error does not vary with Mach number at Mach numbers up to 0.90. By combining the constant position error of the fuselage with the error due to the airspeed head the calibration was extended to a Mach number of 0.85. For the data presented in this paper

at Mach numbers above 0.85 and at Mach numbers below 0.30, the calibration was extrapolated. This calibration was used throughout the normal-force-coefficient range covered.

The angle-of-attack vane was not calibrated for position error in flight; however, the estimated errors in angle of attack due to position error, boom bending, and pitching velocity were small. The angles of attack presented in this paper have been corrected only for boom bending.

The estimated accuracies of the measured quantities pertinent to this paper are as follows:

Mach number, M	± 0.01
Normal load factor, n	± 0.02
Aerodynamic wing-panel load, L_{WP} , pounds	± 100
Wing-panel bending moment, BM_{WP} , foot-pounds	± 400
Wing-panel pitching moment, PM_{WP} , foot-pounds	± 200
Airplane angle of attack, α_A , degrees	± 0.5

TESTS, RESULTS, AND DISCUSSION

The data presented in this paper were obtained in left and right turns and in lg stall approaches at altitudes from 10,000 feet to 24,000 feet. All of the data presented were obtained with power on and with the landing gear and wing flaps retracted. Data are presented for both slats-locked and slats-unlocked configurations.

The aerodynamic characteristics of the D-558-II wing in the presence of the fuselage are presented in figures 6, 7, and 8. These data are presented as plots of Mach number, slat position, airplane normal-force coefficient, left- and right-wing normal-force coefficient, left- and right-wing bending-moment coefficient, and left-wing pitching-moment coefficient against airplane angle of attack. The data are presented at several Mach numbers for the slats-locked configuration in figure 6 and for the slats-unlocked configuration in figure 7. Data obtained at high normal-force coefficient in stall approaches are presented in figure 8 for the slats-locked and slats-unlocked conditions. For some of the data presented in figures 6 to 8 airplane buffeting was present. In these regions the data represent the mean value of the fluctuating quantity. The normal-force coefficient at which buffeting starts is presented as a function of Mach number in reference 3.

Mach Number Effects

Normal-force-curves slopes.- The variations with Mach number of the slopes of the normal-force-coefficient curves $dC_N/d\alpha_A$ for the wing panels and the airplane are presented in figure 9. The value of $dC_{N_{WP}}/d\alpha_A$ for the wing panel in the presence of the fuselage increases from a value of 0.061 at a Mach number of 0.40 to 0.090 at a Mach number of 0.87. The total airplane normal-force-coefficient-curve slope is approximately 8 percent higher than the wing normal-force-curve slope throughout the Mach number range. This difference is due principally to the fuselage lift. Calculations of the normal-force-curve slope by means of the Weissinger method (reference 8) for the wing panel outboard of the fuselage and for the complete wing assuming that the wing extends to the airplane center line also show that the normal-force-curve slope of the complete wing is about 8 percent higher than that for the wing panel.

Wing bending moments and spanwise centers of pressure.- From the measurements of the wing bending moments and shears the center of pressure of the aerodynamic load on the wing panel can be found. The variation of the wing-bending-moment coefficient $C_{B_{WP}}$ with the wing-panel normal-force coefficient $C_{N_{WP}}$ for several Mach numbers is presented in figure 10. The wing-bending-moment coefficient varies linearly with wing-panel normal-force coefficient and there is little change with Mach number.

If the effects of aileron deflection, rolling velocity, and wing twist are small, the spanwise center of pressure of the additional air load over the wing panel is

$$C.P.A = \frac{y_{WP}}{b_{WP}/2} = \frac{dC_{B_{WP}}}{dC_{N_{WP}}}$$

The variation with Mach number of the additional air-load center of pressure for the wing panels outboard of the 33-inch spanwise station is shown in figure 11. Also shown in figure 11 is the theoretical additional air-load center of pressure calculated by the Weissinger method for the wing panel (reference 7). In calculating the theoretical center of pressure, the aspect ratio and taper ratio of the portion of the wing outboard of the 33-inch spanwise station was used. The experimental center of pressure of the additional air load is approximately 48 percent of the wing-panel semispan and does not change appreciably with Mach number. The theoretical spanwise center of pressure is located at 44.3 percent of the wing-panel semispan.

Wing pitching moments and aerodynamic centers.- From plots of the wing-panel pitching-moment coefficient against wing-panel normal-force coefficient the aerodynamic center of the aerodynamic load on the wing panel may be found. The aerodynamic center of the aerodynamic load on the wing panel is

$$\text{a.c.} = 0.25 - \frac{\partial C_{M_{c_{WP}}}/4}{\partial C_{N_{WP}}}$$

The variation with Mach number of the aerodynamic center of the wing panel is shown in figure 12(a). Also shown in figure 12(a) is the location of the aerodynamic center (23 percent of the wing-panel mean aerodynamic chord) obtained by the Weissinger method. (See reference 7.) The aerodynamic center of the wing panel does not change appreciably at Mach numbers up to 0.80. At Mach numbers between 0.80 and 0.87 the data indicate that the aerodynamic center moves rearward. The aerodynamic center of the wing is located at approximately 24 percent of the wing-panel mean aerodynamic chord at a Mach number of 0.4 and moves forward slightly to about 22 percent at a Mach number of 0.8. From a Mach number of 0.80 to 0.87 the data indicate that the aerodynamic center moves rearward to approximately 30 percent of the wing-panel mean aerodynamic chord.

The values of aerodynamic center shown in figure 12(a) were obtained, in general, at airplane normal-force coefficients less than 0.5. At a constant Mach number there appeared to be some variation of $\partial C_M / \partial C_N$ with normal-force coefficient; however, the data were not consistent enough to obtain the variation of the aerodynamic center with normal-force coefficient throughout the Mach number range. In general, the data indicate that for the slats-locked configuration the wing aerodynamic center does not vary with normal-force coefficient at low normal-force coefficients. At some higher normal-force coefficient the aerodynamic center moves forward somewhat and then at high normal-force coefficients the aerodynamic center moves rapidly rearward. The normal-force coefficient at which the aerodynamic center moves forward appears to decrease with Mach number; for instance, at a Mach number of about 0.4 the aerodynamic center appears to move slightly forward at a wing-panel normal-force coefficient of about 0.7, whereas at a Mach number of 0.7 the aerodynamic center starts to move forward at a wing-panel normal-force coefficient of about 0.3. For the slats-unlocked configuration, the results are similar except that the normal-force coefficient for which the initial forward movement of the aerodynamic center occurs appears to be higher than for the slats-locked configuration.

The variation with Mach number of the aerodynamic center of the wing-fuselage combination was found from the tail loads measurements presented in reference 2. The aerodynamic center of the air load on the fuselage is

$$(\text{a.c.})_F = 0.25 - \left(\frac{\partial C_M}{\partial C_N} \right)_F$$

where

$$\left(\frac{\partial C_M}{\partial C_N} \right)_F = \frac{dC_{N_{WF}}}{dC_{N_F}} \left(\frac{\partial C_M}{\partial C_N} \right)_{WF} - \frac{dC_{N_W}}{dC_{N_F}} \left(\frac{\partial C_M}{\partial C_N} \right)_W$$

The values of $\frac{dC_{N_{WF}}}{dC_{N_F}}$ and $\frac{dC_{N_W}}{dC_{N_F}}$ were found from the data presented in reference 6.

The variation of the aerodynamic center of the wing, fuselage, and wing-fuselage combination with Mach number is shown in figure 12(c). The aerodynamic centers are presented in percent of the mean aerodynamic chord of the complete wing. It can be seen in figure 12(c) that the rearward movement of the wing-fuselage aerodynamic center at Mach numbers up to 0.80 is caused by the rearward movement of the fuselage aerodynamic center with Mach number. The data indicate that the more abrupt rearward movement of the wing-fuselage aerodynamic center above a Mach number of 0.8 is caused by rearward aerodynamic-center movement on the sweptback wing. The variation with Mach number of the aerodynamic center of the fuselage in percent of fuselage length is presented in figure 12(b).

Normal-Force-Coefficient Effects

Bending moments. - The variation of the wing-panel bending-moment coefficient with wing-panel normal-force coefficient at high normal-force coefficients is shown in figure 13. The variation of wing-panel bending-moment coefficient with angle of attack is presented in figure 8.

For the slats-locked configuration the bending-moment coefficient increases almost linearly with angle of attack and wing-panel normal-force coefficient up to an angle of attack of about 10° and a wing-panel normal-force coefficient of about 0.85. At angles of attack and normal-force coefficients above these values the wing bending-moment coefficient remains approximately constant; this constant bending-moment coefficient indicates an inboard movement of the spanwise center of pressure.

For the slats-unlocked configuration the wing bending-moment coefficient increases almost linearly with angle of attack and wing-panel normal-force coefficient at angles of attack up to about 20° and at wing-panel normal-force coefficients up to approximately 1.15. The wing-bending-moment coefficient decreases from an angle of attack of 22° to 24° and then remains almost constant up to an angle of attack of 38° .

Pitching moments.- The variation with wing-panel normal-force coefficient of the wing-panel pitching-moment coefficient based on wing-panel area and wing-panel mean aerodynamic chord is shown in figure 14. The variation of wing-panel pitching-moment coefficient with angle of attack is presented in figure 8. Data are shown in figure 14(a) for the slats-locked configuration and in figure 14(b) for the slats-unlocked configuration.

Figures 8(a) and 14(a) show that, for the slats-locked condition, the wing-panel pitching-moment coefficient decreases abruptly at an angle of attack of about 9° and a wing-panel normal-force coefficient of about 0.85.

In the data for the slats-unlocked configuration (figs. 8(b) and 14(b)) a similar increase in wing-panel stability is indicated at an angle of attack of about 11° and a wing-panel normal-force coefficient of about 0.86.

The variation with airplane normal-force coefficient of the wing-panel pitching-moment coefficient based on one-half of the total wing area and the mean aerodynamic chord of the complete wing is shown in figures 15(a) and 15(b) for the slats-locked and slats-unlocked configurations, respectively. The data have been presented as a function of angle of attack in figures 8(a) and 8(b). The data, when presented in this manner, represent the portion of the complete airplane pitching-moment coefficient contributed by the wing panels outboard of the fuselage. For the slats-locked configuration the contribution of the wing to the airplane pitching moment is stable at airplane normal-force coefficients up to 1.1. An increase in the stability of the wing is indicated at an airplane normal-force coefficient of about 0.88. This increase does not appear to be as abrupt as in figure 14 because the airplane normal-force coefficient increases above the angle of attack at which the wing normal-force coefficient reaches a maximum. The data for the slats-unlocked configuration show that the contribution of the wing to the airplane pitching-moment coefficient is stable at airplane normal-force coefficients up to 1.3. An increase in the stability of the wing is indicated at an airplane normal-force coefficient of about 0.90. At an angle of attack of about 23° and an airplane normal-force coefficient of 1.3 it is indicated that the wing-panel pitching moment increases abruptly and then remains relatively constant at higher angles of attack or airplane normal-force coefficients.

Centers of pressure.- The variations of the chordwise and spanwise centers of pressure with airplane angle of attack, wing-panel normal-force coefficient and airplane normal-force coefficient are presented in figure 16. The data are shown in figure 16(a) for the slats-locked condition and in figure 16(b) for the slats-unlocked condition and are presented as percentages of the wing-panel semispan and the wing-panel mean aerodynamic chord. The centers of pressure shown were obtained from the data of figure 8.

For the slats-locked configuration the spanwise and chordwise centers of pressure are approximately constant at angles of attack up to 8° . At angles of attack from 8° to 27° the spanwise center of pressure moves inboard from approximately 47 percent of the wing-panel semispan to about 41 percent of the semispan. The chordwise center of pressure moves rearward from about 24 percent of the wing-panel mean aerodynamic chord to about 34 percent of the mean aerodynamic chord in the angle-of-attack range.

For the slats-unlocked configuration, the spanwise center of pressure moves gradually outboard and the chordwise center of pressure is about constant at angles of attack up to 10° . At angles of attack from 10° to 22° the spanwise center of pressure moves outboard from 48 percent to 53 percent of the wing-panel semispan and the chordwise center of pressure moves rearward from 25 percent to 37 percent of the wing-panel mean aerodynamic chord. At an angle of attack of about 23° the spanwise center of pressure shifts inboard to about 45 percent of the semispan and the chordwise center of pressure moves forward to about 32 percent of the mean aerodynamic chord and then does not change appreciably at angles of attack up to 38° .

Effect of the wing and fuselage on the longitudinal stability of the airplane at high normal-force coefficients.- The effect of the wing and fuselage on the stability of the airplane is shown in figures 17(a) and 17(b) as plots of elevator angle, wing pitching-moment coefficient, fuselage pitching-moment coefficient, and wing-fuselage pitching-moment coefficient against airplane angle of attack and normal-force coefficient for the slats-closed configuration. The wing-fuselage pitching moments were determined from the tail-load measurements presented in references 2 and 6. The fuselage pitching moments were determined by subtracting the wing pitching moments from the wing-fuselage pitching moments.

The variation of elevator angle with angle of attack and normal-force coefficient shown in figure 18 indicates that the airplane is stable at angles of attack up to 9° and airplane normal-force coefficients up to 0.8. At angles of attack above 9° and normal-force coefficients above 0.8 the airplane is unstable. The wing pitching-moment curve shows that the wing is stable throughout the angle-of-attack range covered in figure 17. At an angle of attack of about 9°

and an airplane normal-force coefficient of 0.80 where the airplane becomes unstable, the wing becomes slightly more stable. The fuselage contributes a destabilizing moment except for a small angle-of-attack range between 11° and 13° where the variation of fuselage pitching-moment coefficient with angle of attack and airplane normal-force coefficient is stable. Above an angle of attack of 13° and an airplane normal-force coefficient of about 0.93 the fuselage becomes unstable again.

The data of figure 17 show that the instability of the airplane is not caused by the wing or fuselage. In addition, the spanwise center of pressure starts to move inboard at the angle of attack at which the airplane becomes unstable for the slats-locked configuration. (See fig. 16(a).) This center-of-pressure movement is in the direction for an unstable change in downwash at the tail.

SUMMARY OF RESULTS

The results obtained from wing-load measurements on the D-558-II airplane in the Mach number range from 0.37 to 0.87 indicate that:

1. The wing normal-force-curve slope increases from a value of 0.061 at a Mach number of 0.40 to 0.090 at a Mach number of 0.87 and is about 8 percent lower than the airplane normal-force-curve slope throughout the Mach number range.
2. The spanwise center of pressure of the additional air load on the wing is located at approximately 48 percent of the wing-panel semispan and does not vary with Mach number for Mach numbers up to 0.87.
3. The aerodynamic center of the wing is located at approximately 24 percent of the wing-panel mean aerodynamic chord at a Mach number of 0.4 and moves forward slightly to about 22 percent at a Mach number 0.8. From a Mach number of 0.80 to 0.87 the aerodynamic center moves rearward to about 30 percent of the wing-panel mean aerodynamic chord.
4. The rearward movement of the aerodynamic center of the wing-fuselage combination with Mach number at Mach numbers up to 0.80 is caused by a rearward movement of the aerodynamic center of the fuselage with Mach number. The increase in the stability of the airplane with Mach number in this Mach number range, therefore, may be partly attributed to the rearward movement of the fuselage aerodynamic center with Mach number.

5. For the slats-locked configuration the center of pressure on the wing moves inboard and rearward at high angles of attack. For the slats-unlocked configuration the center of pressure moves outboard and rearward at high angles of attack up to an angle of attack of 23° . At an angle of attack of 23° the center of pressure moves abruptly inboard and forward and then remains approximately at the same position at angles of attack up to 38° .

6. The wing does not cause the longitudinal instability of the airplane at high normal-force coefficients since the wing becomes more stable in the angle-of-attack range for which the airplane is unstable.

Langley Aeronautical Laboratory
National Advisory Committee for Aeronautics
Langley Field, Va.

REFERENCES

1. Sjoberg, S. A.: Flight Measurements with the Douglas D-558-II (BuAero No. 37974) Research Airplane. Static Lateral and Directional Stability Characteristics as Measured in Sideslips at Mach Numbers up to 0.87. NACA RM L50C14, 1950.
2. Mayer, John P., Valentine, George M., and Mayer, Geraldine C.: Flight Measurements with the Douglas D-558-II (BuAero No. 37974) Research Airplane. Determination of the Aerodynamic Center and Zero-Lift Pitching-Moment Coefficient of the Wing-Fuselage Combination by Means of Tail-Load Measurements in the Mach Number Range from 0.37 to 0.87. NACA RM L50D10, 1950.
3. Mayer, John P., and Valentine, George M.: Flight Measurements with the Douglas D-558-II (BuAero No. 37974) Research Airplane. Measurements of the Buffet Boundary and Peak Airplane Normal-Force Coefficients at Mach Numbers up to 0.90. NACA RM L50E31, 1950.
4. Wilmerding, J. V., Stillwell, W. H., and Sjoberg, S. A.: Flight Measurements with the Douglas D-558-II (BuAero No. 37974) Research Airplane. Lateral Control Characteristics as Measured in Abrupt Aileron Rolls at Mach Numbers up to 0.86. NACA RM L50E17, 1950.
5. Stillwell, W. H., Wilmerding, J. V., and Champine, R. A.: Flight Measurements with the Douglas D-558-II (BuAero No. 37974) Research Airplane. Low-Speed Stalling and Lift Characteristics. NACA RM L50G10, 1950.
6. Mayer, John P., and Valentine, George M.: Flight Measurements with the Douglas D-558-II (BuAero No. 37974) Research Airplane. Measurements of the Distribution of the Aerodynamic Load among the Wing, Fuselage, and Horizontal Tail at Mach Numbers up to 0.87. NACA RM L50J13, 1950.
7. DeYoung, John: Theoretical Additional Span Loading Characteristics of Wings with Arbitrary Sweep, Aspect Ratio, and Taper Ratio. NACA TN 1491, 1947.

TABLE I
DIMENSIONS AND CHARACTERISTICS OF THE
DOUGLAS D-558-II AIRPLANE

Wing:

Root airfoil section (normal to 0.30 chord)	NACA 63-010
Tip airfoil section (normal to 0.30 chord)	NACA 63 ₁ -012
Total area, sq ft	175.0
Span, ft	25.0
Mean aerodynamic chord, in.	87.301
Root chord (parallel to plane of symmetry), in.	108.51
Tip chord (parallel to plane of symmetry), in.	61.18
Taper ratio	0.565
Aspect ratio	3.570
Sweep at 0.30 chord, deg	35.0
Incidence at fuselage center line, deg	3.0
Dihedral, deg	-3.0
Geometric twist, deg	0
Total aileron area (aft of hinge), sq ft	9.8
Aileron travel (each), deg	±15
Total flap area, sq ft	12.58
Flap travel, deg	50

Horizontal tail:

Root airfoil section (normal to 0.30 chord)	NACA 63-010
Tip airfoil section (normal to 0.30 chord)	NACA 63-010
Area (including fuselage), sq ft	39.9
Span, in.	143.6
Mean aerodynamic chord, in.	41.75
Root chord (parallel to plane of symmetry), in.	53.6
Tip chord (parallel to plane of symmetry), in.	26.8
Taper ratio	0.50
Aspect ratio	3.59
Sweep at 0.30 chord line, deg	40.0
Dihedral, deg	0
Elevator area, sq ft	9.4
Elevator travel, deg	
Up	25
Down	15
Stabilizer travel, deg	
Leading edge up	4
Leading edge down	5

[REDACTED]

TABLE I
DIMENSIONS AND CHARACTERISTICS OF THE
DOUGLAS D-558-II AIRPLANE - Concluded

Vertical tail:

Airfoil section (parallel to fuselage center line),	NACA 63-010
Area, sq ft	36.6
Height from fuselage center line, in.	98.0
Root chord (parallel to fuselage center line), in.	146.0
Tip chord (parallel to fuselage center line), in.	44.0
Sweep angle at 0.30 chord, deg	49.0
Rudder area (behind the hinge line), sq ft	6.15
Rudder travel, deg	±25

Fuselage:

Length, ft	42.0
Maximum diameter, in.	60.0
Fineness ratio	8.40
Speed-retarder area, sq ft	5.25

Power plant J-34-WE-40
2 jets for take-off

Airplane weight (full fuel), lb 10,645

Airplane weight (no fuel), lb 9,085

Airplane weight (full fuel and 2 jets), lb 11,060

Center-of-gravity locations:

Full fuel (gear down), percent mean aerodynamic chord	25.3
Full fuel (gear up), percent mean aerodynamic chord	25.8
No fuel (gear down), percent mean aerodynamic chord	26.8
No fuel (gear up), percent mean aerodynamic chord	27.5
Full fuel and 2 jets (gear down), percent mean aerodynamic chord	29.2



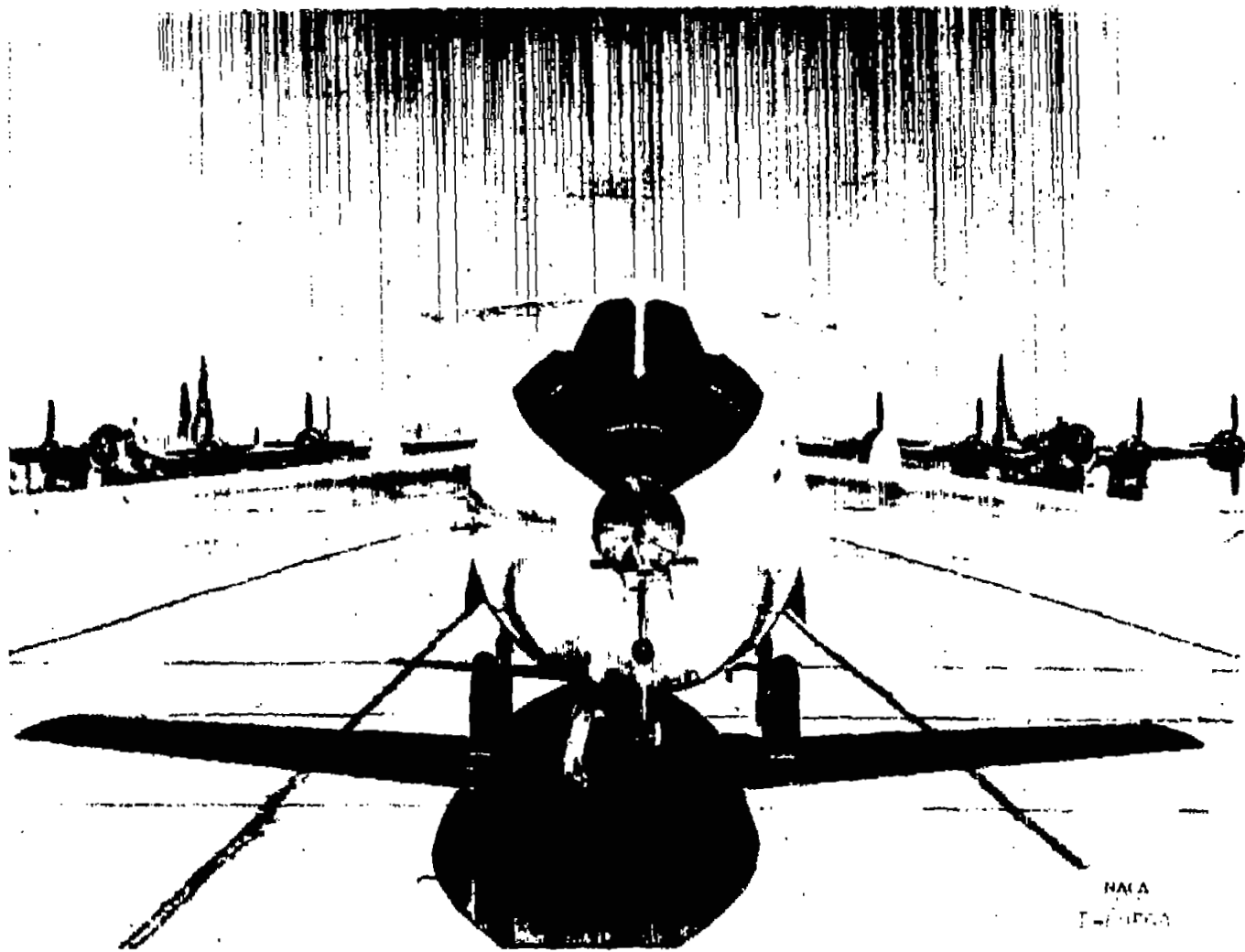


Figure 1.- Front view of Douglas D-558-II (BuAero No. 37974) research airplane.



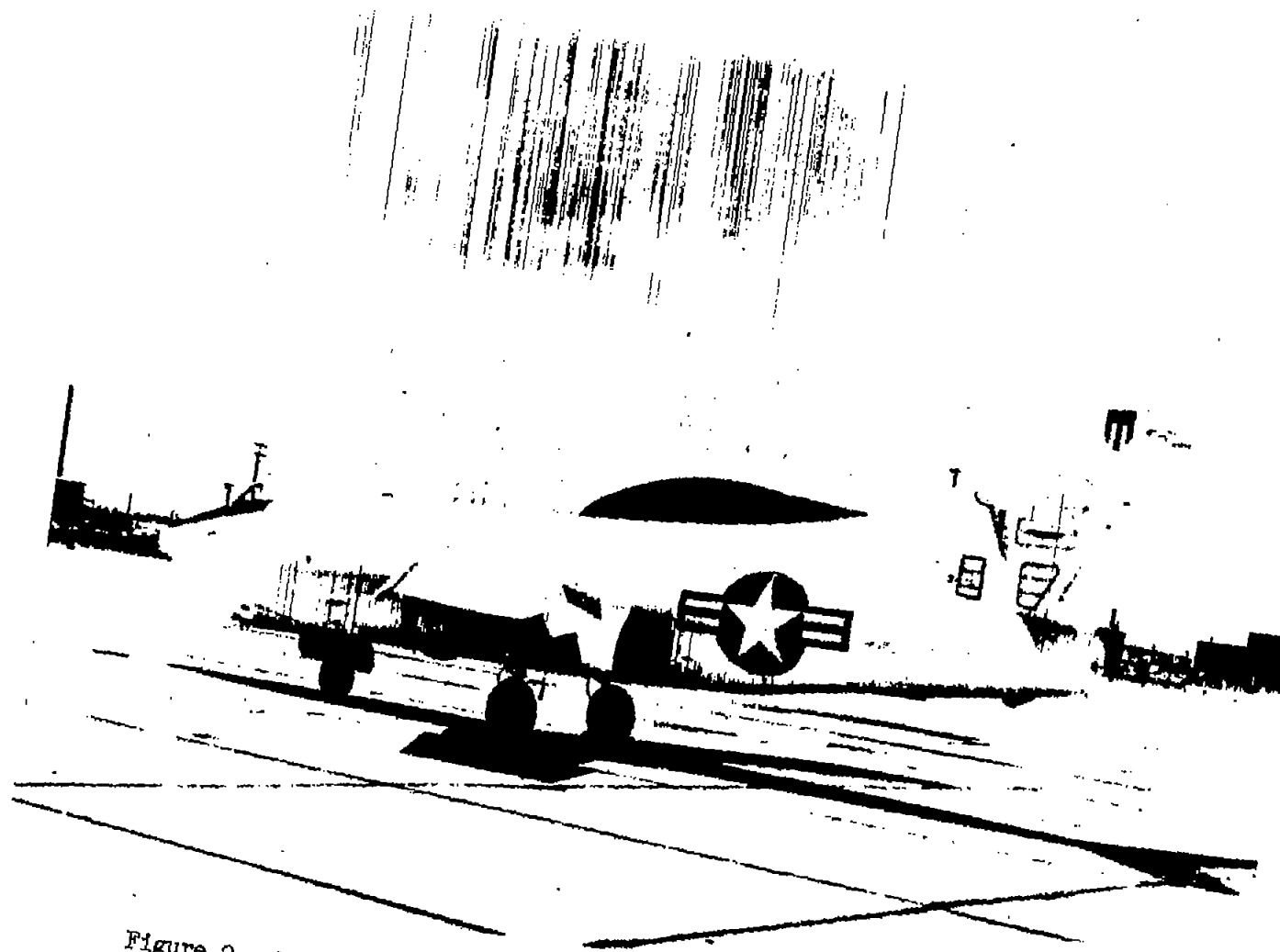


Figure 2.- Three-quarter rear view of Douglas D-558-II (BuAero No. 37974) research airplane.



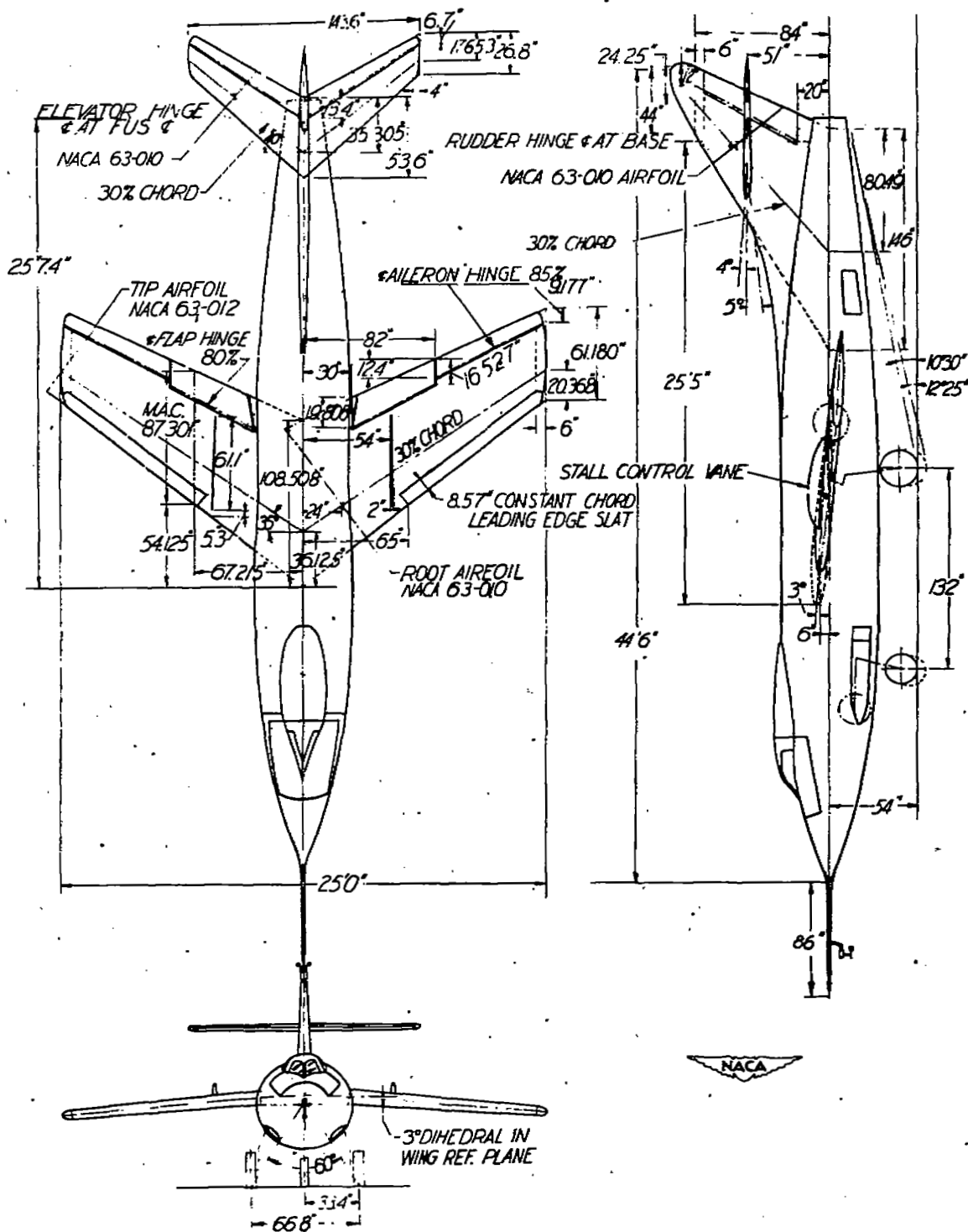


Figure 3.- Three-view drawing of the Douglas D-558-II (BuAero No. 37974) research airplane.

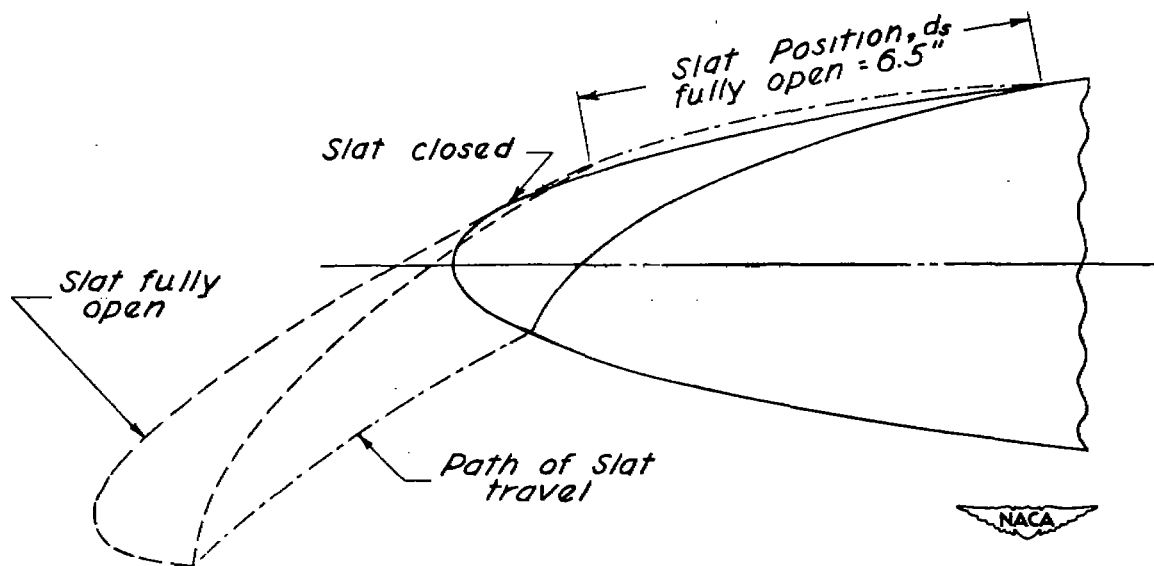


Figure 4.- Section of wing slat of Douglas D-558-II (BuAero No. 37974) research airplane perpendicular to leading edge of wing.

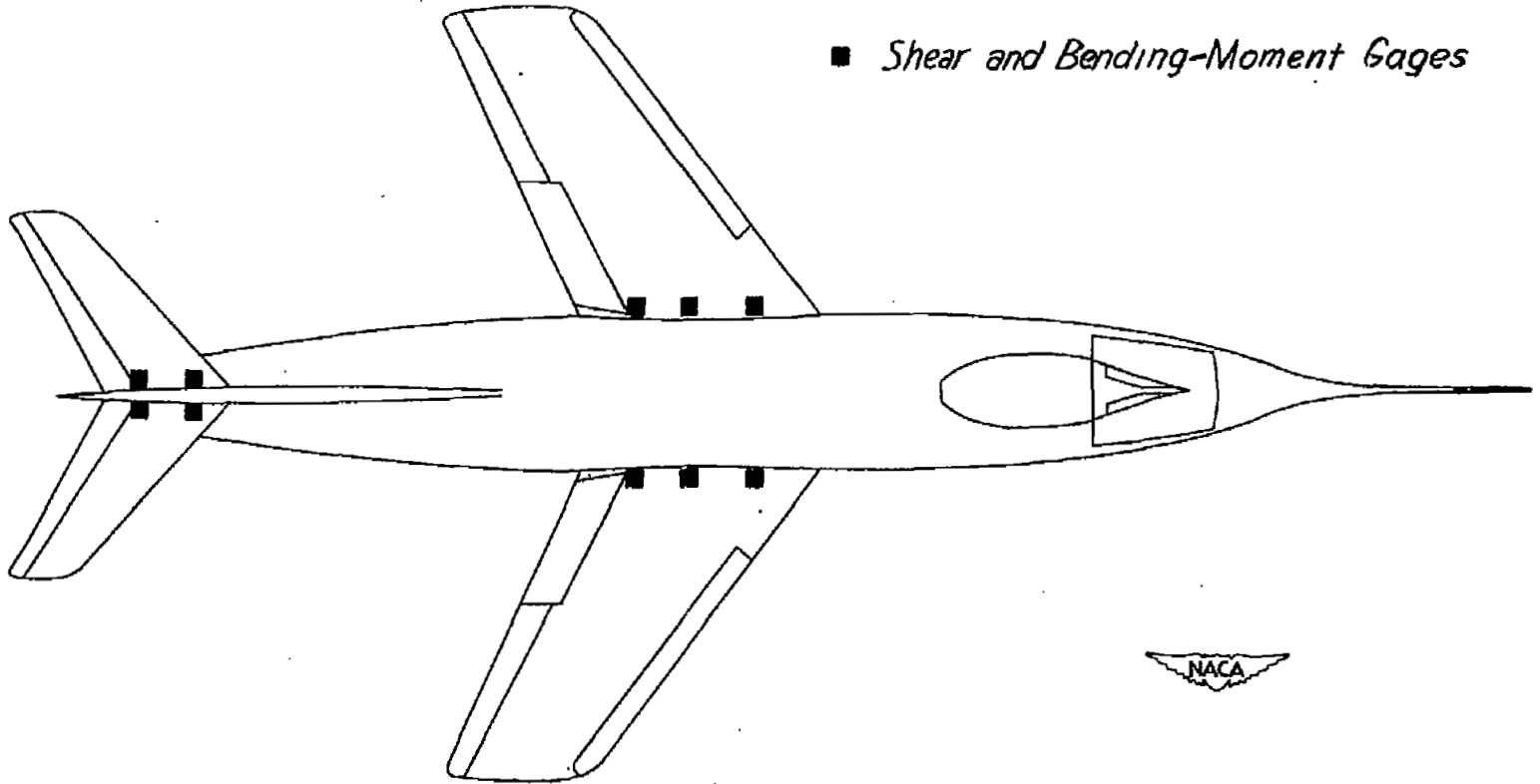


Figure 5.- Locations of strain gages on the Douglas D-558-II (BuAero No. 37974) research airplane.

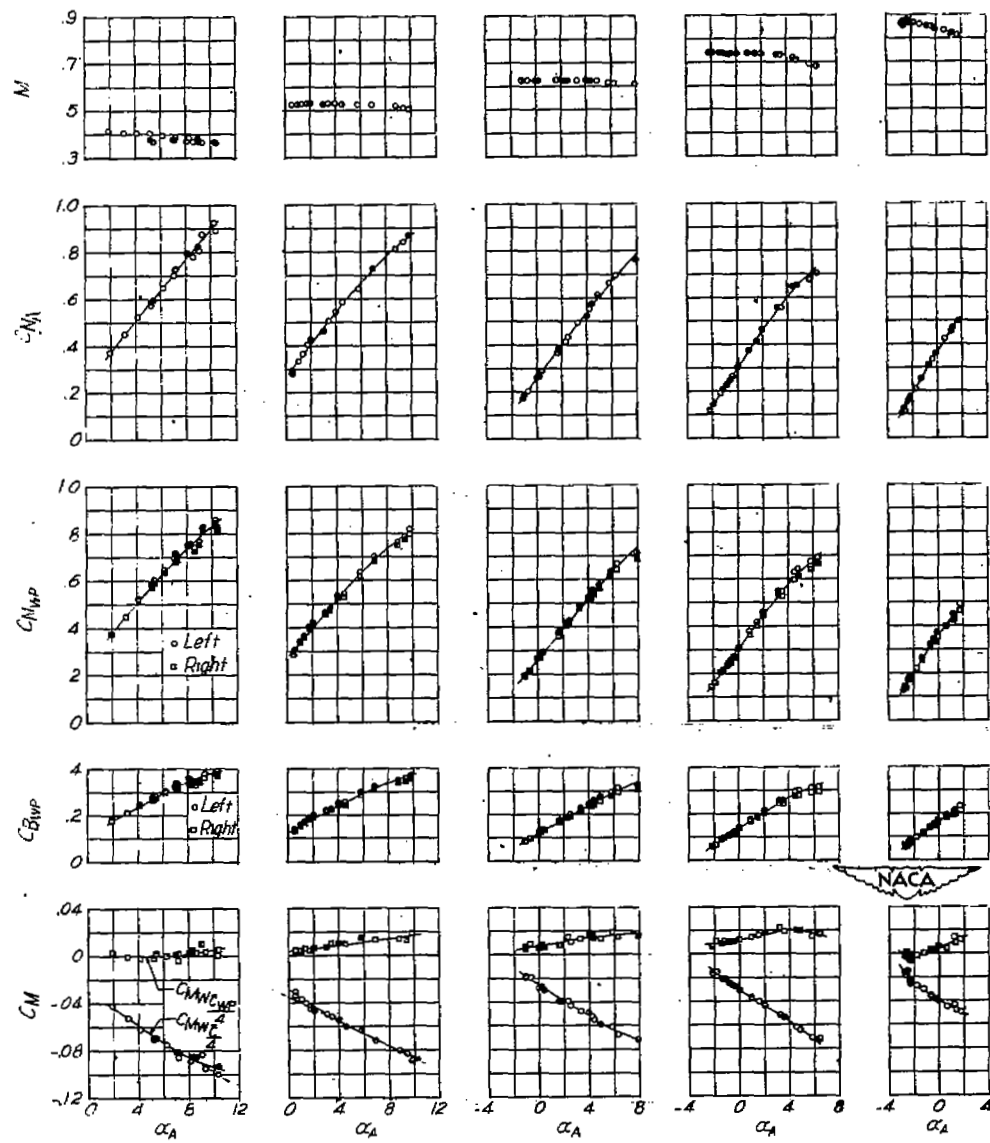


Figure 6.- Aerodynamic characteristics of the wing. Slats locked.

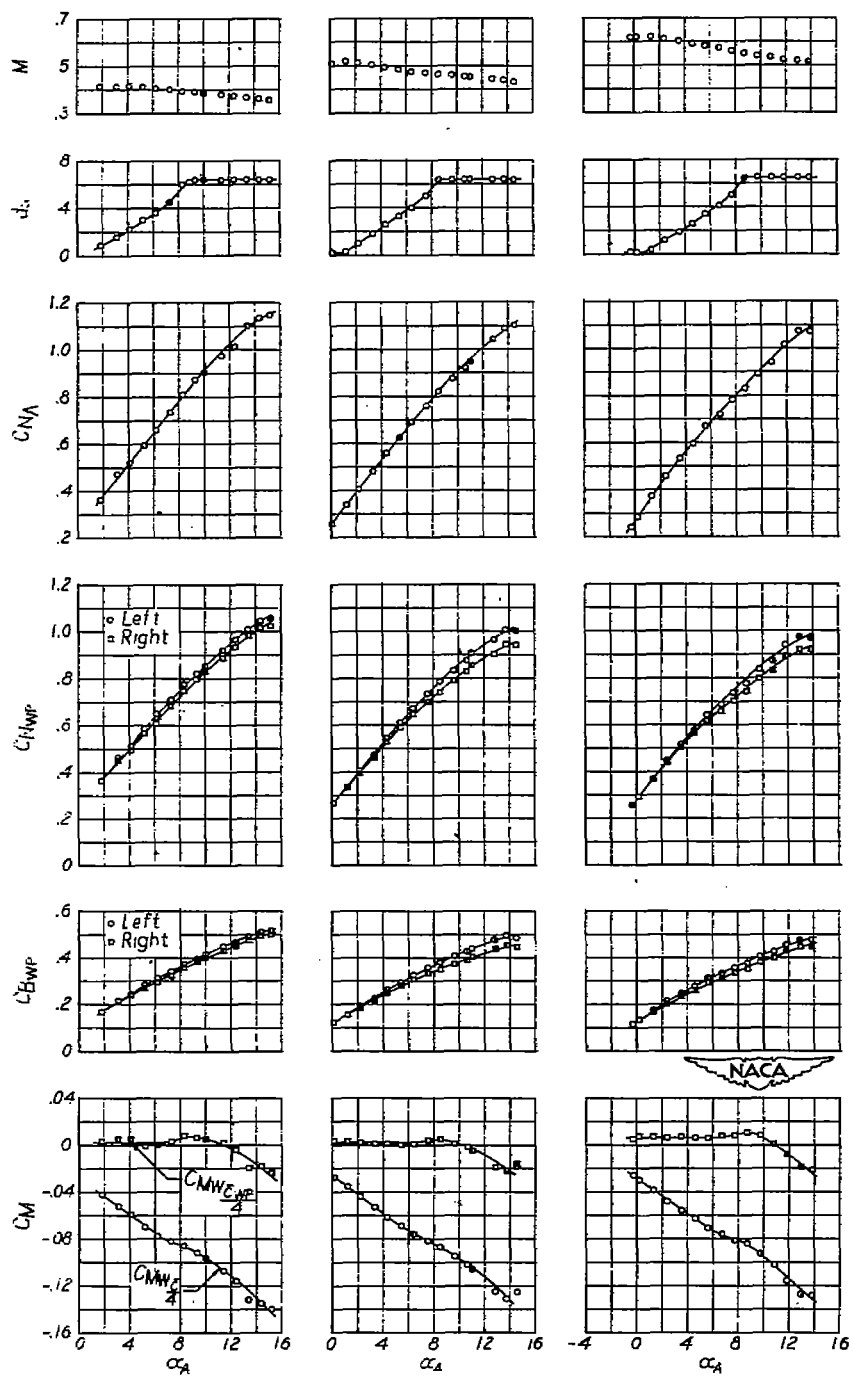
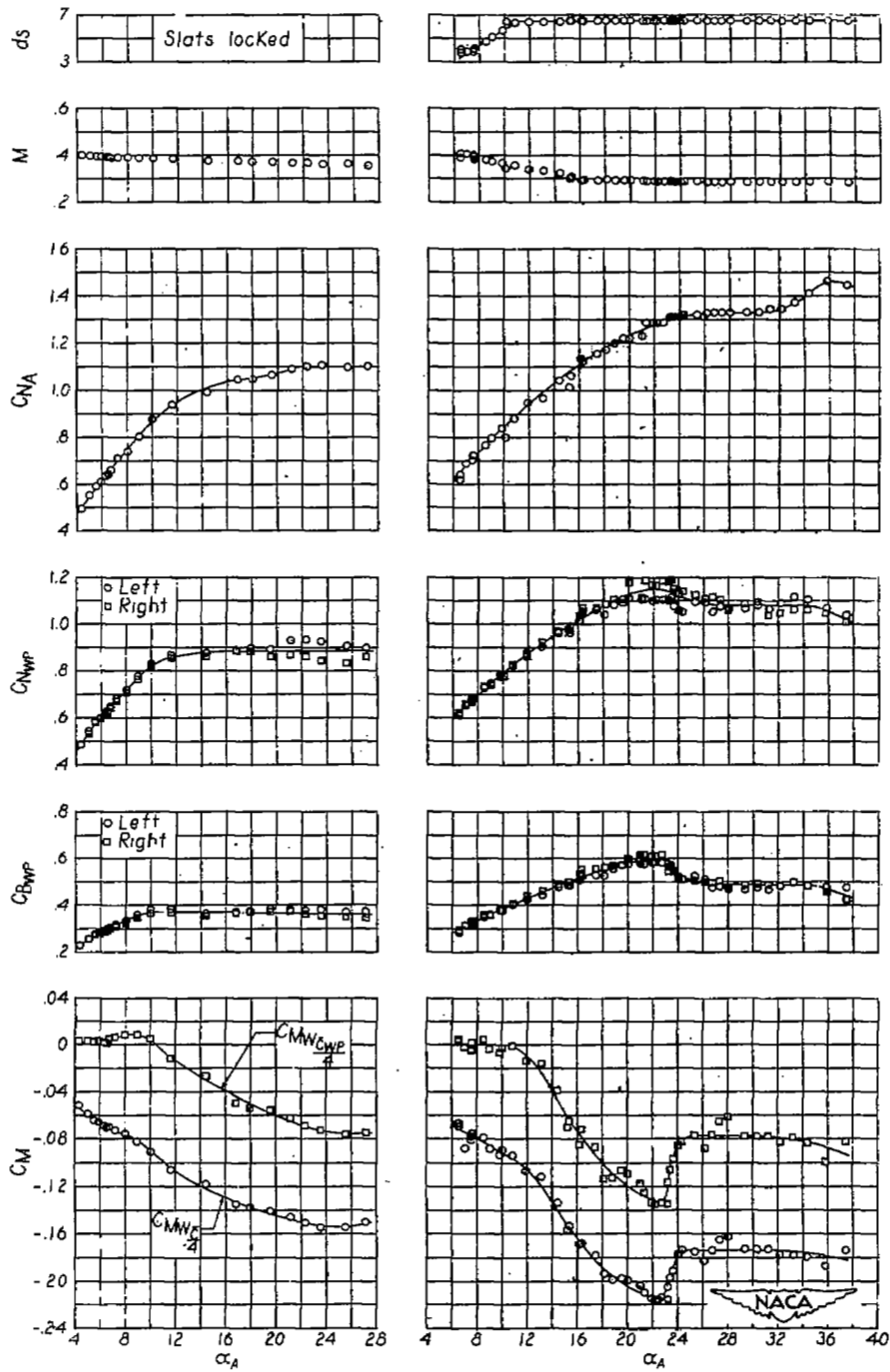


Figure 7.- Aerodynamic characteristics of the wing. Slats unlocked.



(a) Slats locked.

(b) Slats unlocked.

Figure 8.- Aerodynamic characteristics of the wing at high angles of attack.

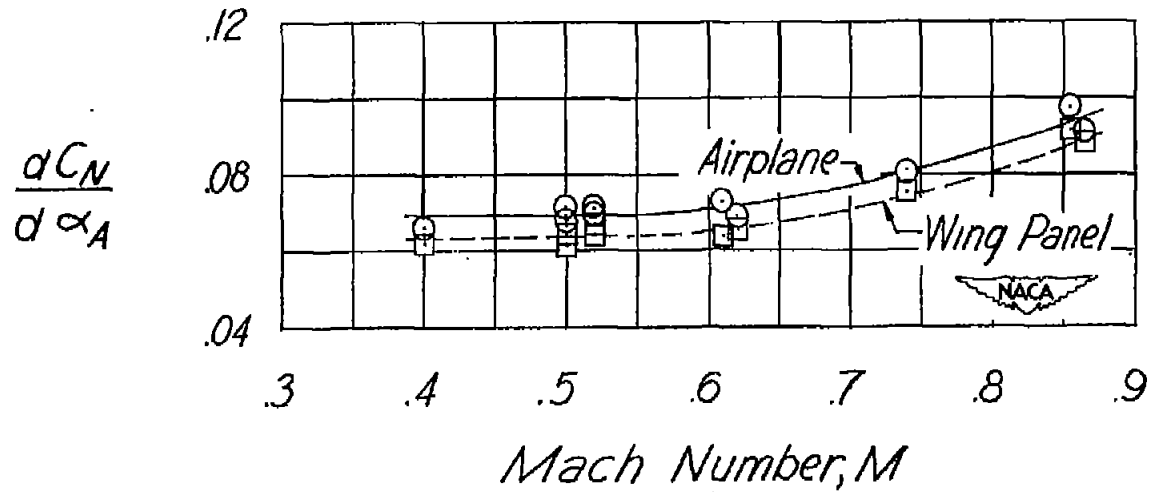


Figure 9.- Variation of the normal-force-curve slope with Mach number for the complete airplane and for the wing in the presence of the fuselage.

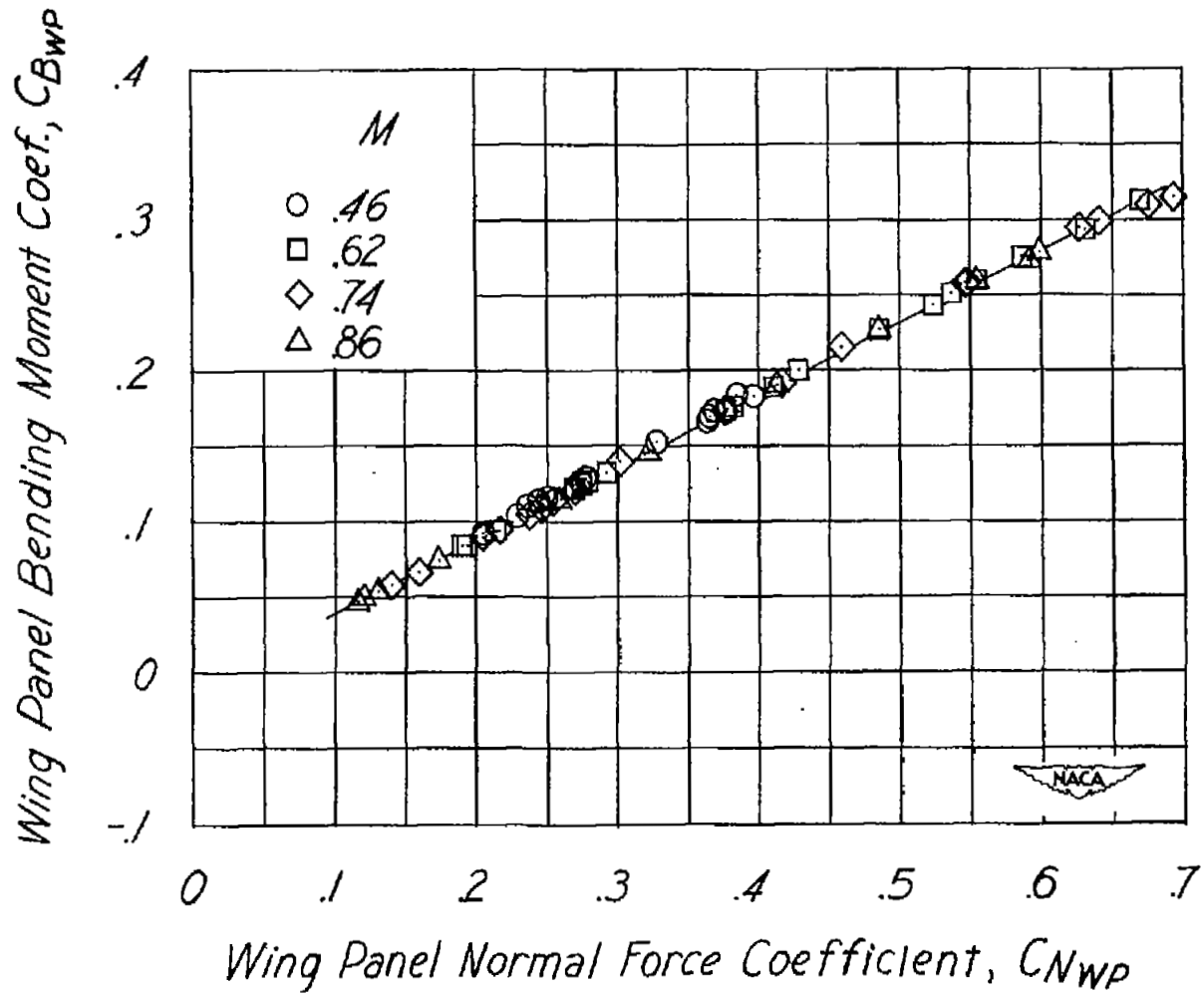


Figure 10.- Variation of wing-panel bending-moment coefficient with wing-panel normal-force coefficient.

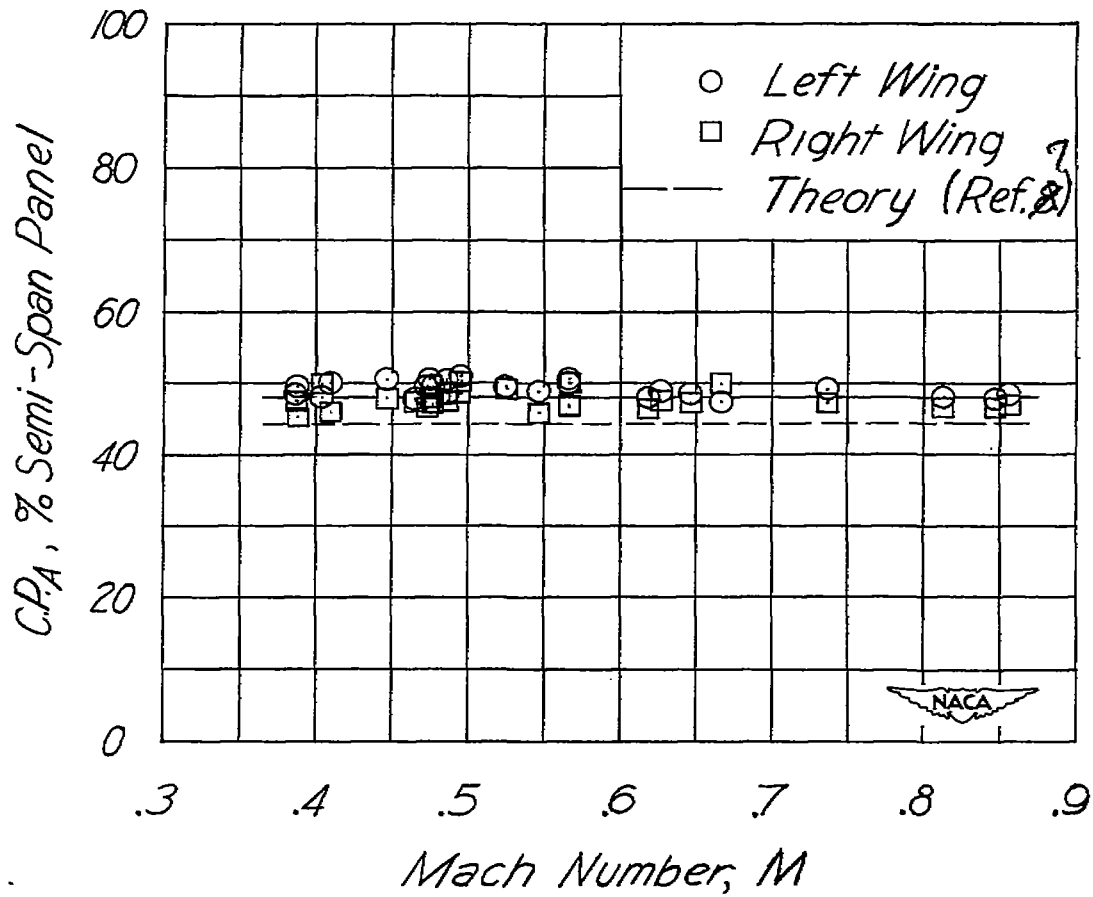


Figure 11.- Variation with Mach number of the spanwise center of pressure of the additional air load.

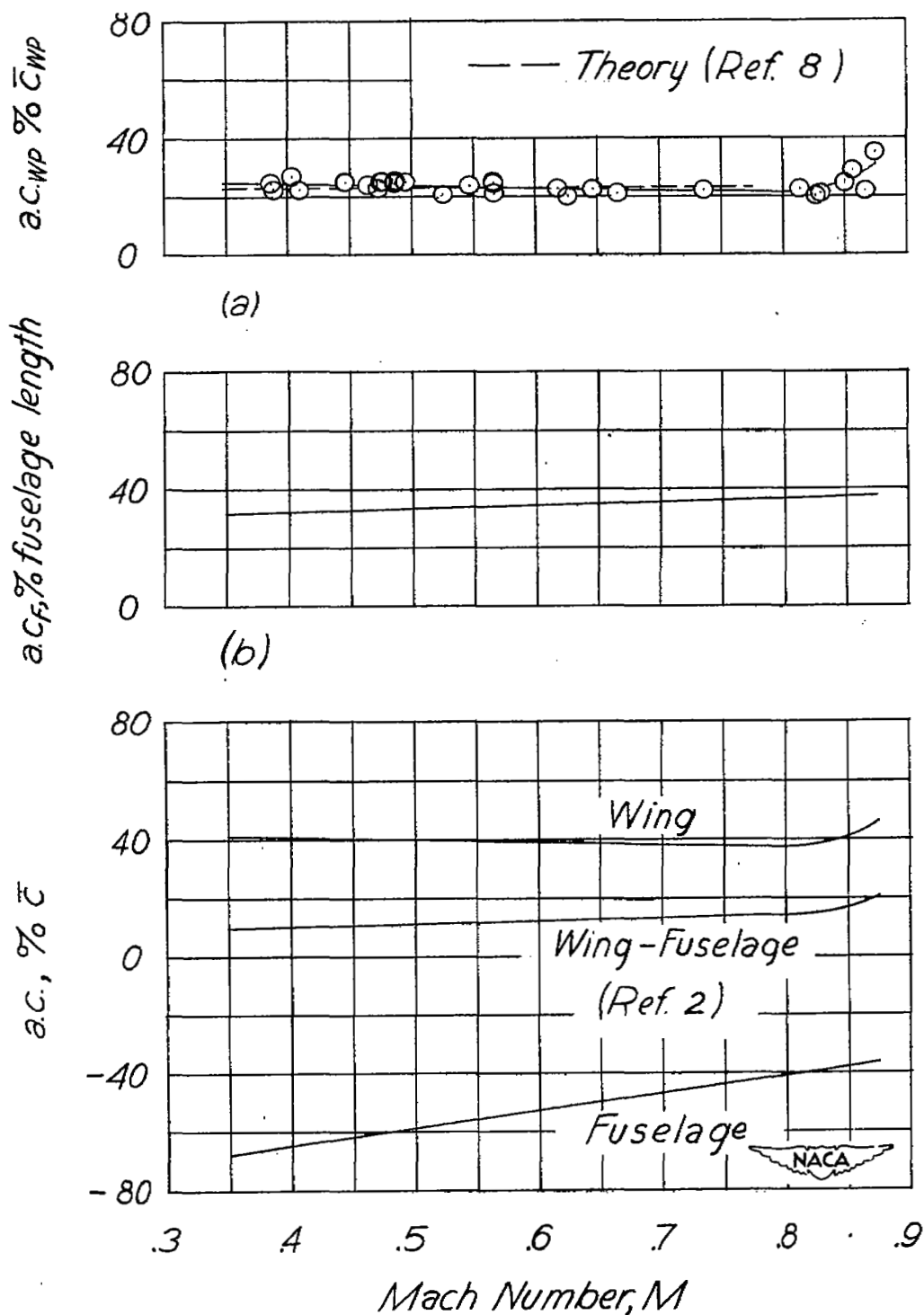
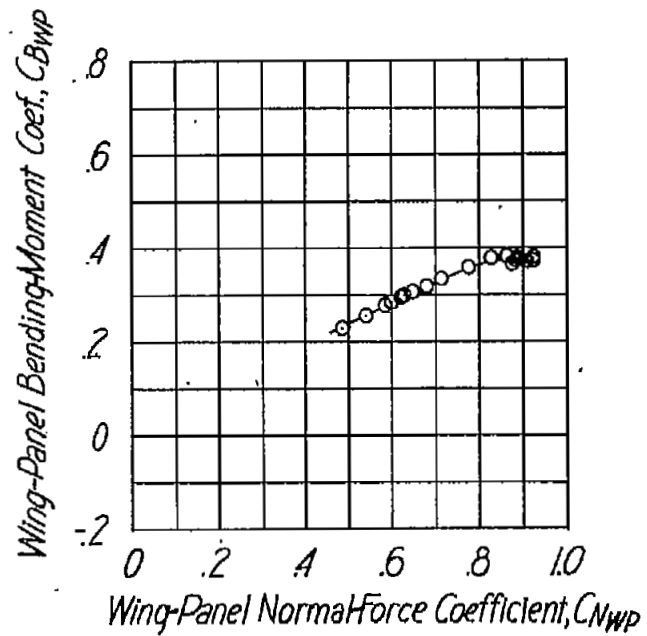
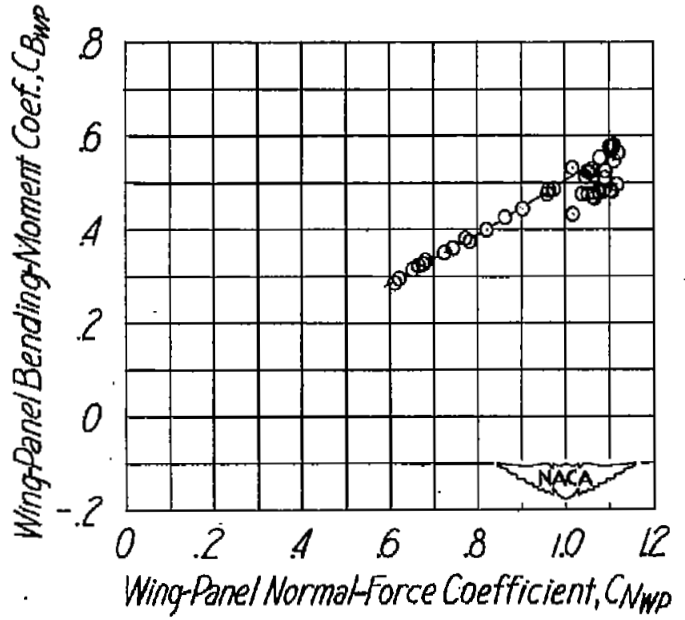


Figure 12.- Variation with Mach number of the aerodynamic center of the wing, fuselage, and wing-fuselage combination.

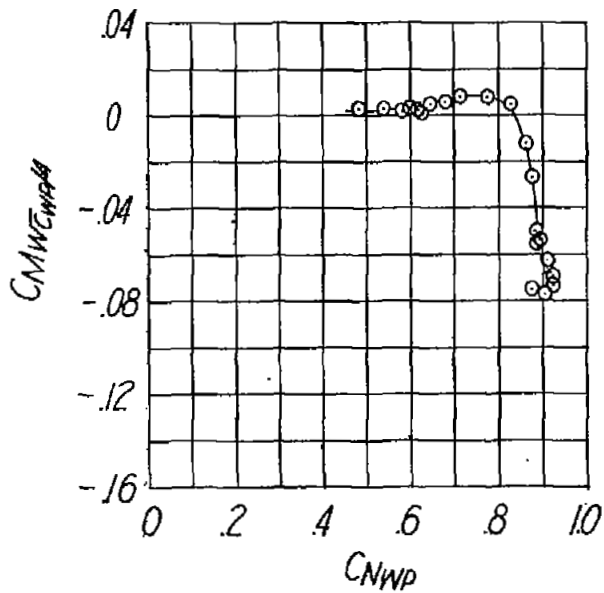


(a) Slats locked.

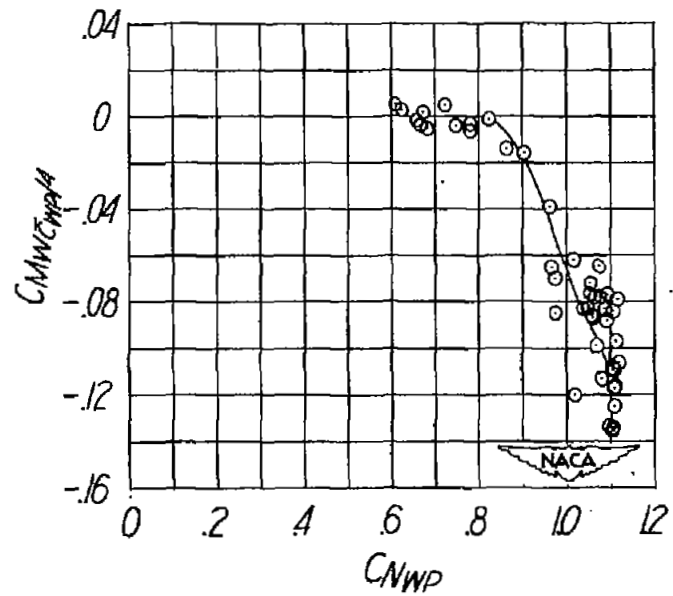


(b) Slats unlocked.

Figure 13.- Variation of wing-panel bending-moment coefficient with wing-panel normal-force coefficient at high normal-force coefficients.

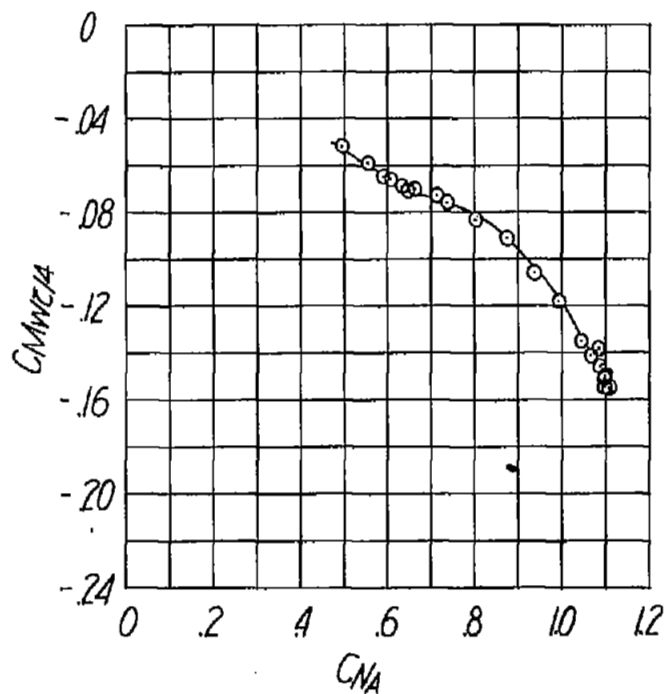


(a) Slats locked.

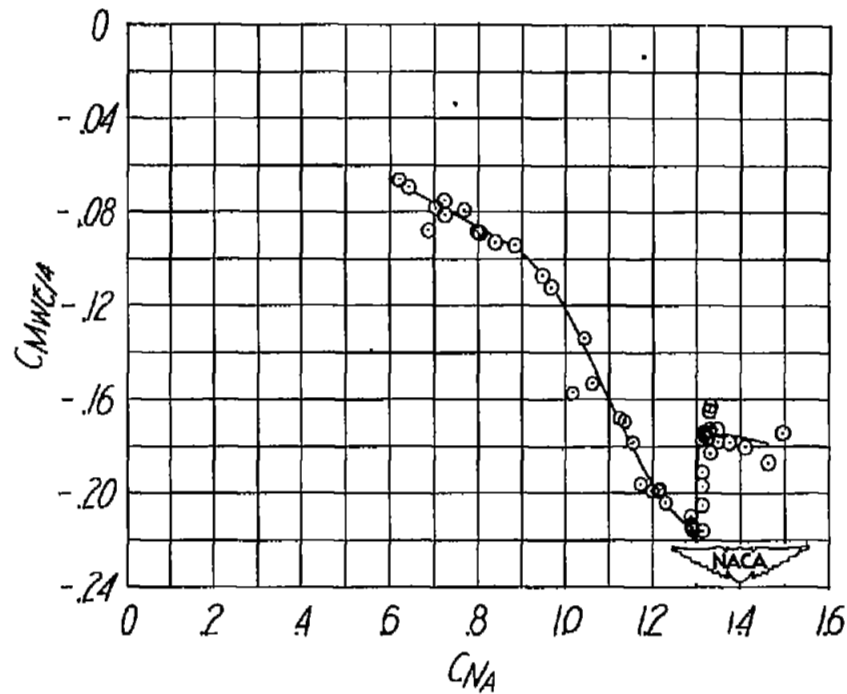


(b) Slats unlocked.

Figure 14.- Variation of wing-panel pitching-moment coefficient C_{m_w}/C_{WPA} with wing-panel normal-force coefficient at high normal-force coefficients.

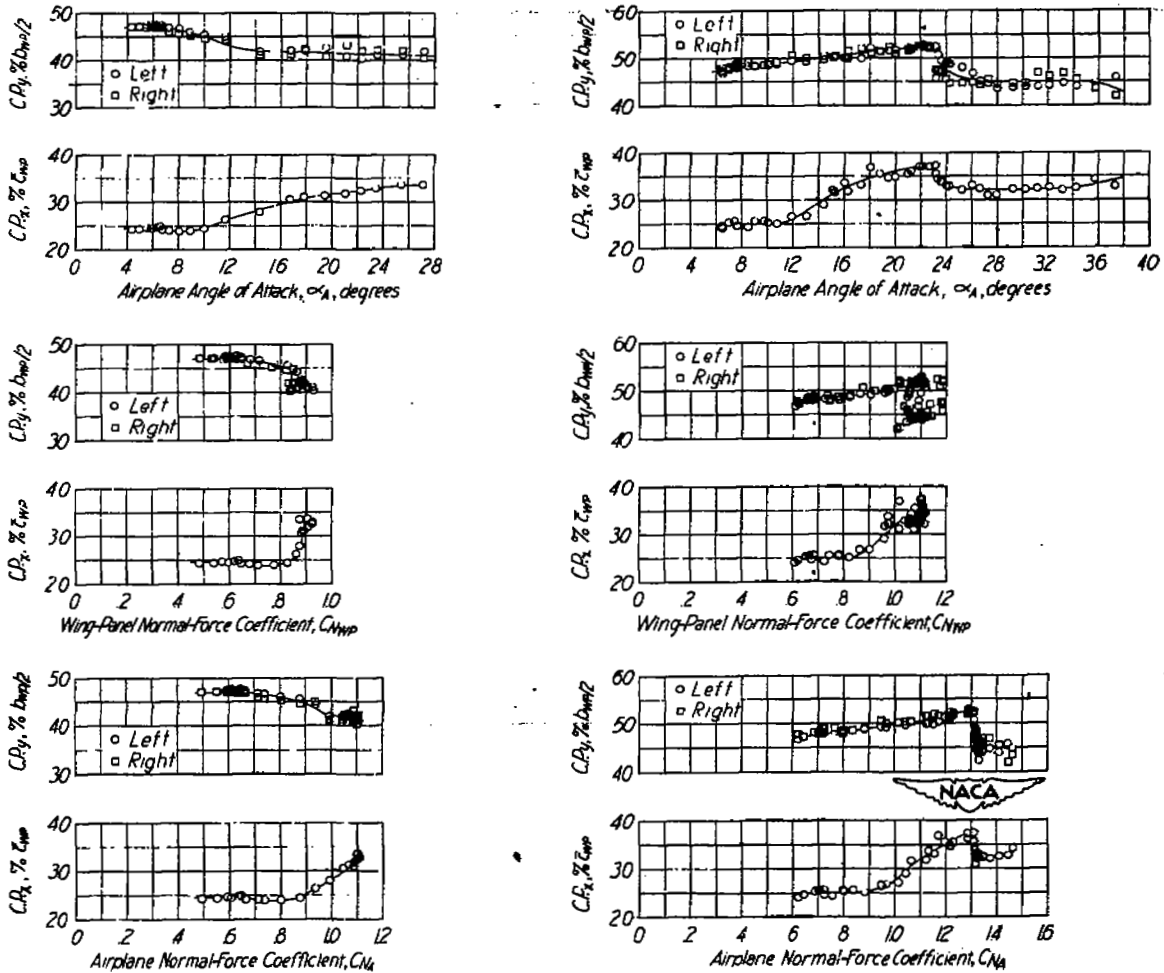


(a) Slats locked.



(b) Slats unlocked.

Figure 15.- Variation of wing-panel pitching-moment coefficient $C_{M_{W/C/4}}$ with airplane normal-force coefficient at high normal-force coefficients.



(a) Slats locked.

(b) Slats unlocked.

Figure 16.- Wing chordwise and spanwise centers of pressure.

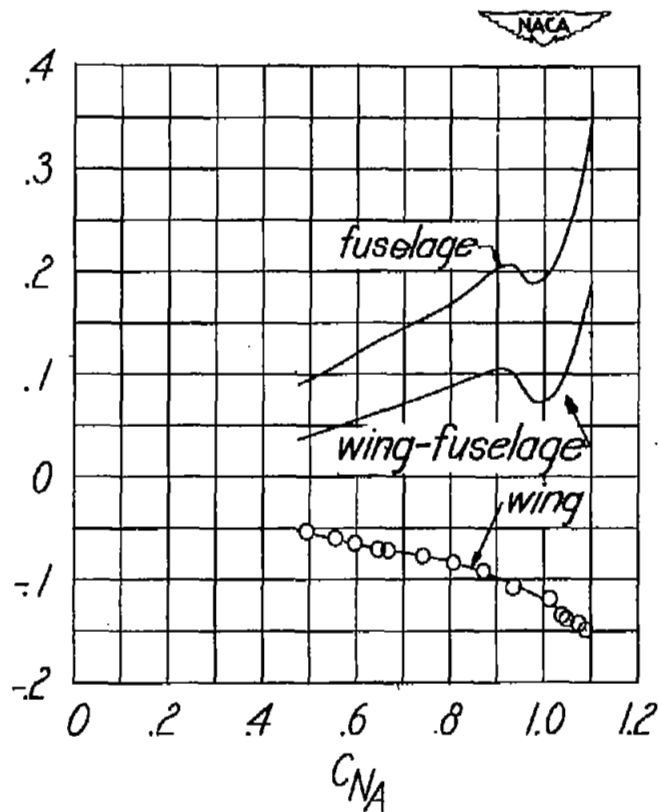
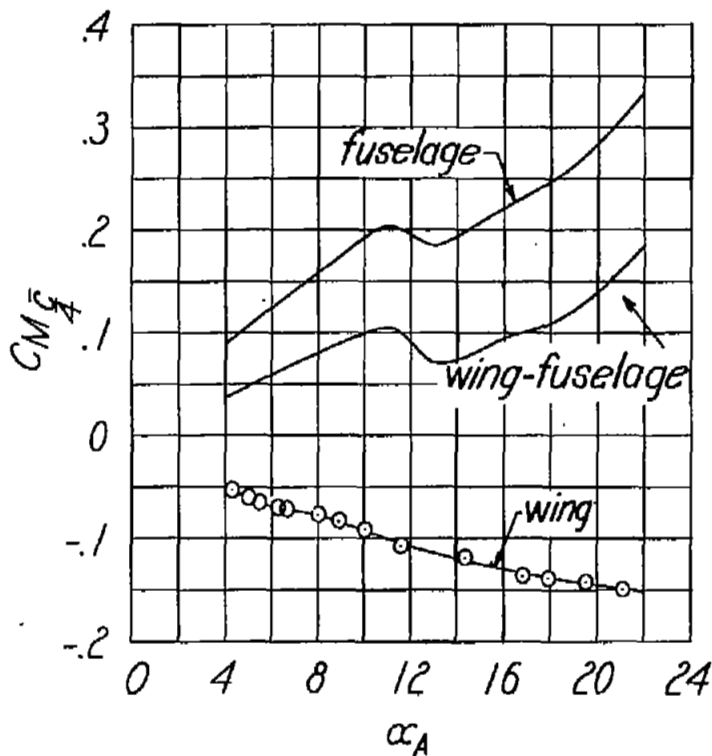
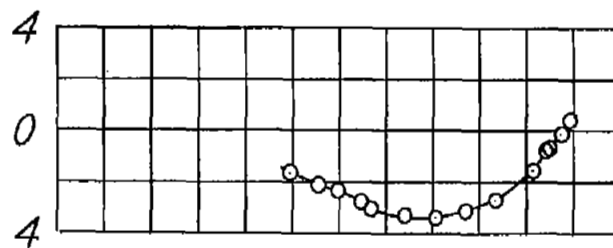
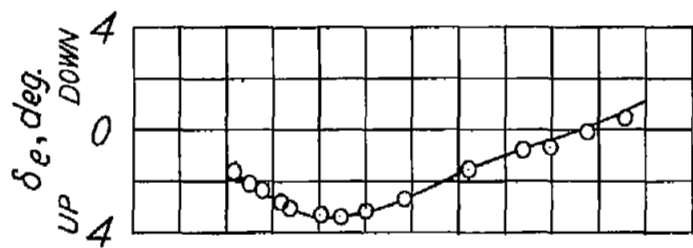


Figure 17.- Effect of wing and fuselage on the airplane longitudinal stability.

NASA Technical Library



3 1176 01436 8097